ARTICLE

Received 00th January 20xx,

Accepted 00th January 20xx

DOI: 10.1039/x0xx00000x

Multiplexed elemental bioimaging with quadrupole ICP-MS and high-frequency laser ablation systems.

Thomas E. Lockwood,[a] Mika T. Westerhausen [a] and David P. Bishop* [a]

The advent of fast washout and high Hz rate laser ablation systems has reduced blurring and greatly improved the throughput of analyses performed using laser ablation-inductively coupled plasma-mass spectrometry (LA-ICP-MS). However, historical laser syncronisation issues have limited the number of elements aquired in a single run when using quadrupole-based ICP-MS. Aliasing noise results from incorrect synronisation between the MS acquistion time and laser firing rate and is made more preventlent by fast washout cells. Oversampling at high Hz is a possible solution to aliasing, yet remains unexplored for the context of multiplexed elemental bioimaging. In this paper we determine the minimum laser firing rates required to prevent aliasing for any MS dwell time and provide an equation for calculating aliasing noise. The effects of oversampling were explored using simulations and the ablation of gelatine standards and murine brains. Higher firing rates were found to reduce aliasing and increase signal, but increased the risks of sample damage and raised backgrounds. Aliasing was found to be insignificant at firing rates and dwell times greater than 200 Hz and 2 ms for a typical (20 ms full-width at 10% of maximum) fast washout cell. At these parameters, the noise from aliasing was overwhelmed by noise from other sources and synchronisation was a non-issue. This allowed facile selection of acquistion and dwell times to increase the number of targeted elements or favour those with low sensitivity. Nine elements were collected in a single analysis of a murine brain at 25 pixels per second with no visible aliasing. Use of these parameters will greatly increase throughput and multiplexing capabilities when using high frequency laser ablation with quadrupole-based ICP-MS.

Introduction

Laser ablation-inductively coupled plasma-mass spectrometry (LA-ICP-MS) is a technique used to perform elemental analysis on solid samples. One application of LA-ICP-MS is elemental-bioimaging, an imaging technique that is used to determine the spatial distribution of elements in biological samples. Due to its high sensitivity and quantitative capacity, it has been used to investigate endogenous and exogenous elements for several diseases such as muscular dystrophy,[1] Wilson's disease,[2] and Alzheimer's disease.[3] Traditionally, laser ablation systems had long washout times (>1 s) as large diameter tubing (1/8 inch internal) was used for coupling to an ICP-MS. The limitations of this setup were outlined by Lear et al, who described a relationship between the laser spot size, the laser scan speed, and the total ICP-MS integration time.[4] The laser scan speed could not be more than four times that of the spot size before blurring of the pixels occurred.

LA-ICP-MS imaging quality is affected by two main types of system artefacts: blurring from insufficient washout, and aliasing produced by unsynchronised ablation frequency to sampling time. Blur is the result of overlapping plume volumes between consecutive ablation shots, as the flow is too slow to evacuate the ablation cell of distinct ablated masses. The solution to blurring is improving mass transfer to the plasma which is currently achieved through high speed ablation cell design,[5] sample introduction devices[6] or a combination of both.[7] This is an active area of research with the newest cell designs using double inlet gas flows containing helium and argon to maximise outlet flow.[5,8] Commercial retailers of "fast washout" laser ablation systems, use combination systems in their highest end offerings, with companies advertising single digit millisecond washout times.[6,7,9] While fast washout cells solve the issue of blurring, they can make aliasing problems more severe.

Aliasing is an issue for scanning-type ICP-MS instruments and is caused by incorrect synchronisation of the MS acquisition time and firing rate of the laser.[10] Each laser pulse creates a plume of ablated material that is extracted from the ablation chamber and transported to the ICP-MS. Without synchronisation, the peak of the resulting ion-flux will arrive at different times during the MS dwell time, causing variation in the accumulation of signal. The resulting image is then marred by vertical 'aliasing' or stripes that hinder data interpretation. To ensure synchronisation of the MS and laser, it is recommended that the firing rate f_{LA} of the laser be an integer multiple ($\mathbb{Z}$) of the of the total MS acquisition time f_{MS}, i.e. $\mathbb{Z} = f_{LA} \cdot f_{MS}$.[11] Post processing of data can also be used to reduce aliasing by averaging signal intensities but results in a loss of image

[a] *Hyphenated Mass Spectrometry Laboratory, University of Technology Sydney, Ultimo, Sydney, NSW, Australia.*
[b] *Address here.*
[c] *Address here.*
† Footnotes relating to the title and/or authors should appear here.
Electronic Supplementary Information (ESI) available: [details of any supplementary information available should be included here]. See DOI: 10.1039/x0xx00000x

resolution.[12] The issue of aliasing is so prevalent that it has led to the development of a commercial device to synchronise firing of the laser with the measurement cycle of the mass spectrometer, although it has yet to be used in a published work.[13]

The development of fast washout ablation cells has coincided with the increased access and affordability of high frequency lasers. While previously only excimer lasers could achieve firing rates greater than 100 Hz,[14] current generation LA-ICP-MS imaging systems commonly uses solid-state laser with at least 100 Hz ablation pulse frequencies,[15,16] and up to 1 kHz.[17] The high Hz, fast washout lasers also provide rapid movement of the ablation cell of up to 25 mm/s with 10 nm precision. The majority of previous work on aliasing was performed on low frequency instruments.[11,12] As such, users of these new generation systems with quadrupole-based ICP-MS have adhered to the procedures established for the limitations of slow washout or low firing rate lasers. Slow scan speeds relative to spot size,[18,19] or a limited number of targeted elements were used in anticipation of synchronisation-based aliasing. While quadrupole instruments cannot achieve the multi-elemental pixel acquisition rates of a ToF, these parameters still underutilise the capabilities of new generation lasers.

Laser ablation is a destructive technique, and re-analysis for multiple elements on the same section is not possible. Diseased tissue is often characterised by the change in concentration of multiple elements,[20] and screening for even the most common toxic metals requires the acquisition of many elements. The rarity of the samples and the multi-element roles makes the simultaneous acquisition of multiple elements essential. In addition to endogenous elements, the conjugation of metal analytes to antibodies enables the in-situ imaging of biomarkers. By tagging multiple antibodies with unique isotopes many biomarkers can be simultaneously imaged. Multiplexing analyses has the advantages of providing a wider diagnostic panel and better interrogating disease via the interactions of multiple biomarkers.[21] Unlike fluorescent equivalents, imaging using LA-ICP-MS can acquire a large number of possible simultaneous tags (i.e., isotopes), without requiring unmixing.

The major difficulties of multiplexed analyses by LA-ICP-MS are the low abundances of certain biomarkers and the broad range of possible targets. The mass analysers typically used for LA-ICP-MS, the standard quadrupole and time of flight (ToF),[22,23] have advantages and disadvantages relating to limits of analysis, simultaneous isotope measurement and interferences.[24] Quadrupole mass analysers are limited in the number of targets due to the previously described issues, and the comparatively low sensitivity of ToF detectors limits the analysis of low abundant biomarkers, even with lanthanide tags.[25] This is particularly relevant when the difference in concentration between healthy and diseased tissues is small. While approaches do exist to increase ToF sensitivity,[26] the ability to analyse many elements using a quadrupole would unlock low cost, highly available ICP-MS systems for multiplexed imaging at increased pixel acquisition rates.

While synchronisation is important at the low firing rates common on older generation LA systems, its importance may be overstated for new generation instruments.[10,27] Currently, the majority of users of fast washout LA systems are either using ToF mass analysers for simultaneous data collection, or limiting the analysis to single elements with a quadrupole-based ICP-MS. Here we describe how synchronisation can be mitigated for the fast, multi-element analysis using fast-washout LA coupled to a quadrupole-ICP-MS.

Experimental

Materials

Elemental standards (1000 µg mL^{-1}) and Seastar Baseline nitric acid (HNO_3) used for calibration and cross-quantification were supplied by Choice Analytical (Thornleigh, New South Wales, Australia). Tris-HCl (pH 7.4), ethylenediaminetetraacetic acid (EDTA), and gelatine from porcine skin (300 Bloom, Type A) were purchased from Sigma-Aldrich (Castle Hill NSW, Australia). The mouse brain tissue sections were acquired from the Howard Florey Institute of Neuroscience and Mental Health, University of Melbourne, under the following Howard Florey Animal Ethics Committee approval 15-104-FINMH. Briefly, male C57BL/6 mice were raised according to standard animal care protocols and fed normal chow and water ad libitum. An overdose of sodium pentobarbitone (100 mg kg^{-1}) were used to euthanise the animals and perfused with 30 mL of warmed (37 °C) 0.1 M phosphate buffered saline (PBS), pH 7.4. Tissue was fixed in 4% paraformaldehyde in PBS until the brains sank, after which they were immersed overnight in two changes of 30% sucrose in PBS. The brain tissue was then frozen at -80 °C and mounted in O.C.T.™ via the medulla oblongata and upper spinal cord. After equilibrating at -20 °C, the brains were sectioned using PTFE-coated cryotome blades (DT315R50 Silver Microtome Blades. C. L. Sturkey, Inc., Lebanon PA) on a Cryostar cryotome (CryoStar™, Thermo Fisher Scientific, North Ryde, NSW, Australia) to 30 µm thickness at 90 µm intervals and mounted on standard microscope slides.

Experiments performed on Yttrium-spiked gelatine (1000 ppm), and standards (Mn, Fe, Cu, Zn) used for quantification were prepared according to a previously validated protocol.[28] Briefly, 100 mg of porcine gelatine powder was spiked with metal solutions and made up to 1 ml using a 100 mM tris and 10 mM EDTA buffer solution. The gelatine solution was vortexed and heated at 50 C until dissolved and pipetted into pre-heated slides with HybriWell™ (Sigma-Aldrich) sealing systems attached. Slides were frozen at -80 °C for 5 minutes, the sealing system removed and then dried in a desiccator overnight.

Instrumentation

An Elemental Scientific Lasers imageBIO266 laser ablation system (Kenelec Scientific, Mitcham, Victoria, Australia) coupled to an Agilent Technologies 7900 Series ICP-MS (Agilent Technologies, Mulgrave, Victoria, Australia) was used for all experiments.

Simulations and processing

Simulations of ion flux and detector signals were performed using a custom Python script (available in the ESI). Peak shapes of ablations and subsequent washout were modelled using a log-normal distribution with a full-width at 10% of maximum(FW0.1M) equal to that of the experimentally determined cell washout. Ion flux was modelled as the sum of these peaks, at a millisecond resolution. MS signals were simulated as the sum of ion flux for a defined dwell time.
LA-ICP-MS data was spatially resolved and quantified using external calibration on in-house developed software (Pew^2).[29]

Results and discussion

The current generation of laser ablation systems are capable of fire rates exceeding several hundred hertz and are equipped with ms washout ablation chambers. These fast washout cells have excellent signal to noise properties, as ablation events are delivered to the ICP over a shorter period. However, the short washout presents additional challenges for use with quadruple ICP-MS (ICP-Q-MS). ICP-Q-MSs can only measure a single mass-to-charge at a time, and multi-element analyses require scanning through individual elements, each with their own settling and measurement times. As the total acquisition time decreases, mass transition and settling times take up an increasingly large fraction of the analysis. With typical settling times of around 2 ms, a cell with a 5 ms washout could collect a maximum of 2 elements across a single ablation event when the MS acquisition time is equal to the firing rate. This can be remedied by 'oversampling', firing the laser multiple times during each MS integration period. If the laser firing rate is much faster than the cell washout time, then the ablation of material approaches a steady state.

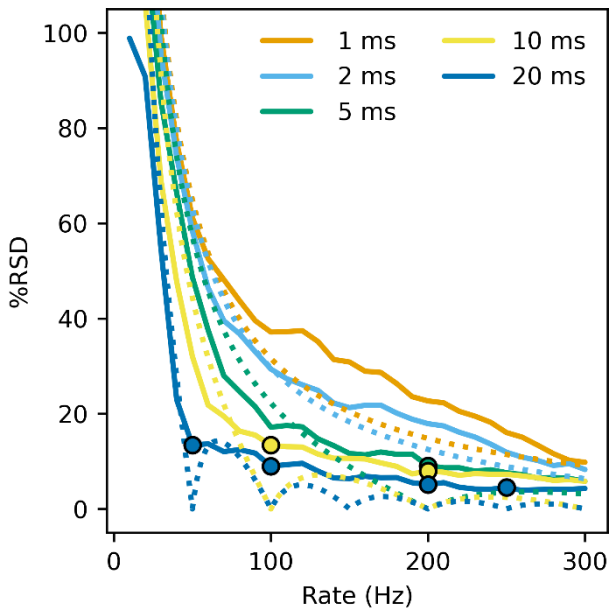

Figure 2. Signal-to-noise of a Y spiked gelatine standard ablated at different firing rates and MS dwell times, using a 40 ms FW0.01M washout ablation chamber. Synchronised parameters are highlighted with circles and predictions from the sawtooth approximation are displayed as dotted lines.

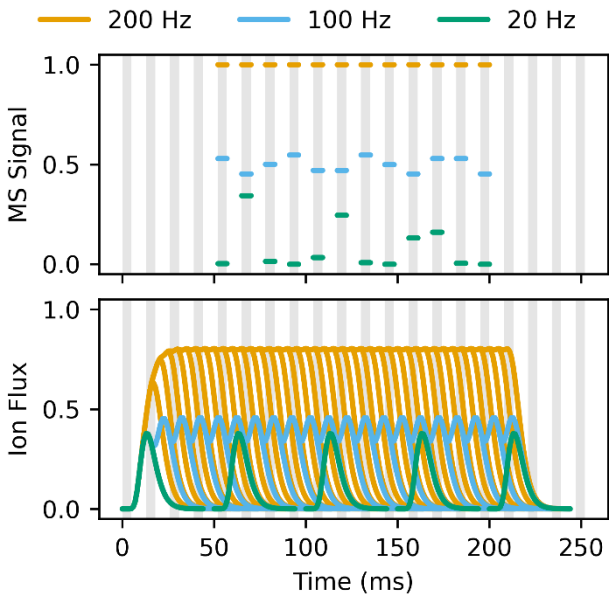

Figure 1. Simulated ion-flux and integrated signals for a 20 ms (FW0.1M) washout cell at three different laser firing rates. Grey regions indicate a single elements dwell time (5 ms; total acquisition of 13 ms). Aliasing is present in the 20 and 100 Hz MS signals, but not at the higher firing rate.

Figure 1 shows a simulation of the analysis of two elements (with a total acquisition time of 13 ms using a 20 ms (FW0.1M) washout cell and non-synchronised MS and laser parameters. As predicted by van Elteren et al.,[11] there is significant aliasing with the laser fire rate at 20 and 100 Hz, with standard deviations in the MS signal of 32 and 7%, respectively. However, only a negligible amount of aliasing (<0.01%) was observed with the laser fire rate at 200 Hz as the ablation of material has reached a steady state. For this particular experiment rates above 200 Hz will remove aliasing. However, the firing rate required to produce a steady state of ablation depends on both the cell washout and MS dwell times.
By assuming the signal produced by steady state ablation is approximately a sawtooth wave, we can predict the maximum error from mis-synchronisation. Equations 1 and 2 calculated the minimum and maximum integrations of the sawtooth for a period $T = f d_t$, where f is the laser firing rate in Hz and d_t is the MS acquisition time in s. The maximum error is then scaled in equation 3 (where $\lfloor x \rfloor$ and $\lceil x \rceil$ represent the floor and ceiling operators) to the amount of steady state ripple using f and the full width washout time, W. These equations can be used to predict the amount of 'ripple' produced during steady state ablation, such as in Figure 1.

$$A_{min} = \frac{(T-\lfloor T \rfloor)^2 - \lfloor T \rfloor}{2} \quad (1)$$

$$A_{max} = \frac{\lceil T \rceil - (\lceil T \rceil - T)^2}{2} \quad (2)$$

$$\%RSD = \frac{100}{fW} \frac{A_{max} - A_{min}}{A_{max}} \quad (3)$$

Together these equations allow us to predict the firing rate required to produce an image without aliasing for any set of cell washout and MS dwell times. The minimum required firing rate

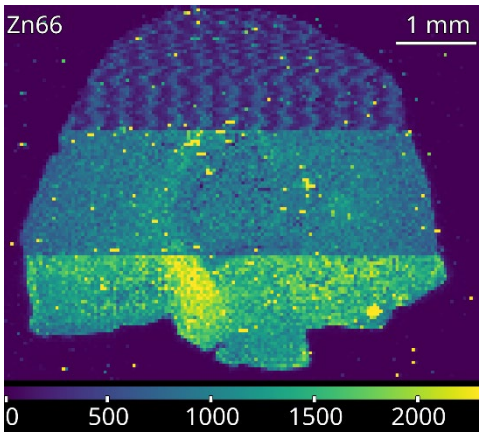

Figure 3. Zn in a murine brain hemisphere imaged at three firing rates. A firing rate of 47, 94 and 188 Hz was used for the top, middle and bottom third of the image, respectively. Aliasing is clearly visible at the lowest firing rate. Firing rates were chosen to minimise synchronisation of the laser and MS.

was calculated for washout and dwell times from 1 to 100 ms, to a maximum of 300 Hz.

To confirm the simulated data, a Yttrium-spiked gelatine standard was ablated at firing rates from 10 to 300 Hz (Figure 2). At low firing rates the noise in ablation is primarily aliasing-based, and the approximation correctly predicts or exceeds overall %RSD. However, at higher Hz the noise from steady state ripple was overwhelmed by sample and instrument noise. The predicted noise (dotted lines) falls below that of the experiment (solid lines). This is further demonstrated by the lack of reduction in %RSD for perfectly synchronised rates (i.e. where there is no offset from an integer value, $\mathbb{Z} \pm 0$). Therefore, when using high-frequency systems for bioimaging aliasing will not be a major source of noise. These results confirm the modelled data that oversampling at high Hz rates to produce a steady signal state mitigates the risks of aliasing. At these rates the benefits of synchronising the laser and MS are negligible and the acquisition time and dwell times of individual elements can be chosen without care, so long as they are above the Hz rate predicted in equation 3.

To demonstrate the benefits of oversampling, a mouse brain was ablated at three laser firing rates: 47, 94 and 188 Hz. Four elements were analysed (Figure S1), with a total MS acquisition time of 0.04 s, corresponding to mismatches of $\mathbb{Z} \pm 0.12$, 0.24 and 0.48 respectively. Other laser parameters and the acquisition time were kept the same across the three experiments. The produced images are recombined in Figure 3 with aliasing due to the mismatched timings visible at the lowest rate, 47 Hz. No aliasing is visible at the higher firing rates, despite larger $\mathbb{Z}$ mismatches. As stated by Van Elteren et al,[27] the requirements for synchronisation relax at higher firing rates, and at least 94 Hz was required to completely eliminate visible aliasing without any dwell or acquisition time considerations. Based on the modelling data, 200 Hz was chosen for the remaining experiments to minimise aliasing while also allowing for a fast enough sampling rate for imaging and tissue-friendly laser flux (25 pixels-per-second, 1.6 J cm^{-2}). Elemental intensities increased at higher firing rates, without a corresponding increase in background counts, likely due to the increased sample volume ablated at higher frequencies of the same laser power.

The major drawback of firing rate oversampling is the increased amount of energy delivered to the sample and the possibility of increased background from unwanted ablation of the sample carrier.[16] Glass slides contain percent levels of elements such as

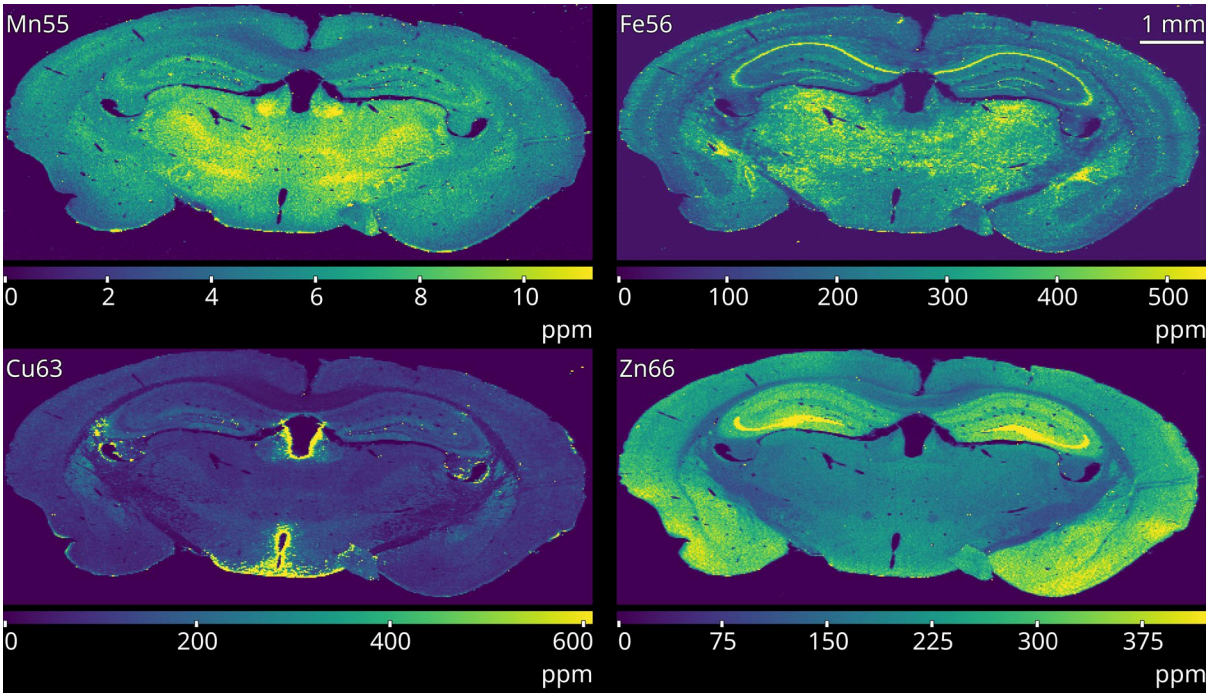

Figure 4. Concentrations (mg kg^{-1}) of four elements in a murine brain, collected using oversampling (200 Hz). A total of nine elements were collected with dwell times ranging from 1 to 6 ms and a total acquisition time of 40 ms. A windowed mean filter (5x5) was used to remove pixels greater than nine standard deviations from the local mean.

Al, Ca, Fe and Mg, and ablation can increase backgrounds and reduce image quality. In our experience, with 266 and 193 nm lasers, glass is not ablated when using low laser powers and high repetition rates. The increased energy also carries the risk of causing sample thermalisation and damage, and testing should be performed to determine an appropriate laser power output for the sample type.[30] Finally, the increases in signal at higher firing rates are only possible when there is sufficient material for ablation.

We tested oversampling for multiplexed imaging by simultaneously acquiring nine elements during imaging of a murine brain (Figure 4). Images were collected at a resolution of 20 µm, scan speed of 500 µm s^{-1} and firing rate of 200 Hz, with the entire experiment taking less than 100 minutes, more than 6 times faster than using the traditional 1:4 spot-size to scan speed ratio. MS dwell times were targeted based on suspected abundance and ranged from 1 ms for high-abundant elements (Na, Mg, K, Ca) to 6 ms for those with lower abundance (Mn, Cu). Concentrations of four elements were determined using spiked gelatine standards and uncalibrated images are available in the ESI (Figure S2). Acquisition of nine elements using a quadrupole ICP-MS is not seen in the literature and is far more than stated to be viable in previous papers exploring high-frequency lasers.[27] These results demonstrate that high quality, multiplexed images can be collected in a very short time using fast-washout, high frequency laser ablation systems.

The dwell and settling times of a quadrupole MS provide a hard limit to the number of elements able to be acquired for any given pixel acquisition rate. The experiments in this paper were performed on a commercial fast washout cell in its default configuration but are applicable to even the newest ultra-fast washout cells (<10 ms FW0.01M). However, the primary benefit of these cells is an extremely high pixel acquisition rates, and this requires MS acquisition times in the milli-seconds. At these acquisition times, a quadrupole instrument must compromise between imaging speed and the number of acquired elements.

Conclusions

Imaging of multiple elements is possible using quadrupole-based ICP-MS and high firing rate lasers to produces high quality images with no visible artefacts. We have determined a method for calculating the appropriate minimum laser firing speed for any combination of ablation cell washouts and MS dwell times. This method was tested using simulated ablation profiles, gelatine standards and tissue. At higher ablation rates the need for synchronisation decreases. Therefore, for typical use, the maximum laser firing rate that can be used without incurring the disadvantages discussed above should be determined by ablation of tissue or a tissue surrogate. Using an ablation cell with a washout greater than 10 ms and firing rate greater than 200 Hz mitigates synchronisation mismatches, and element dwell times greater than a few ms can be chosen indifferently to increase signal for the lower abundant analytes.

Author Contributions

Conceptualised by DPB. Investigation, analysis, and preparation of the original draft was performed by TEL. All authors contributed to writing, review and editing of the manuscript.

Conflicts of interest

There are no conflicts to declare.

Acknowledgements

The authors thank Associate Professor Hare for the donation of the tissue. DPB was supported by the Australian Research Council Discovery Project grant DP230101740.

Notes and references

1 D. P. Bishop, M. T. Westerhausen, F. Barthelemy, T. Lockwood, N. Cole, E. M. Gibbs, R. H. Crosbie, S. F. Nelson, M. C. Miceli and P. A. Doble, *Sci. Rep.*, 2021, **11**, 1–11.
2 S. Weiskirchen, P. Kim and R. Weiskirchen, *Ann. Transl. Med.*, 2019, **7**, S72–S72.
3 B. Paul, D. J. Hare, D. P. Bishop, C. Paton, V. T. Nguyen, N. Cole, M. M. Niedwiecki, E. Andreozzi, A. Vais, J. L. Billings, L. Bray, A. I. Bush, G. McColl, B. R. Roberts, P. A. Adlard, D. I. Finkelstein, J. Hellstrom, J. M. Hergt, J. D. Woodhead and P. A. Doble, *Chem. Sci.*, 2015, **6**, 5383–5393.
4 J. Lear, D. Hare, P. Adlard, D. Finkelstein and P. Doble, *J Anal Spectrom*, 2012, **27**, 159–164.
5 H. a O. Wang, D. Grolimund, C. Giesen, C. N. Borca, J. R. H. Shaw-Stewart, B. Bodenmiller and D. Günther, *Anal. Chem.*, 2013, **85**, 10107–10116.
6 M. A. Reynolds, B. S. Kamber, C. A. McKenna, M. Oelze and S. A. Gleeson, *Am. Mineral.*, 2023, **108**, 18–30.
7 D. N. Douglas, A. J. Managh, H. J. Reid and B. L. Sharp, *Anal. Chem.*, 2015, **87**, 11285–11294.
8 C. Neff, P. Becker and D. Gunther, *J. Anal. At. Spectrom.*, , DOI:10.1039/d1ja00421b.
9 S. J. M. Van Malderen, J. T. van Elteren and F. Vanhaecke, *J Anal Spectrom*, 2014, **30**, 119–125.
10 S. J. M. Van Malderen, J. T. van Elteren, V. S. Šelih and F. Vanhaecke, *Spectrochim. Acta Part B At. Spectrosc.*, 2018, **140**, 29–34.
11 J. T. Van Elteren, V. S. Šelih, M. Šala, S. J. M. Van Malderen and F. Vanhaecke, *Anal. Chem.*, 2018, **90**, 2896–2901.
12 B. Hattendorf, U. Hartfelder and D. Günther, *Anal. Bioanal. Chem.*, 2019, **411**, 591–602.
13 C. A. Norris, L. Danyushevsky, P. Olin and N. R. West, *J. Anal. At. Spectrom.*, 2021, **36**, 733–739.
14 D. Günther and C. A. Heinrich, *J Anal Spectrom*, 1999, **14**, 1369–1374.
15 S. J. M. Van Malderen, T. Van Acker and F. Vanhaecke, *Anal. Chem.*, 2020, **92**, 5756–5764.
16 M. Šala, V. S. Šelih, C. C. Stremtan and J. Teun Van Elteren, *J. Anal. At. Spectrom.*, 2020, **35**, 1827–1831.
17 T. Van Acker, S. J. M. Van Malderen, T. Van Helden, C. Stremtan, M. Šala, J. T. Van Elteren and F. Vanhaecke, *J. Anal. At. Spectrom.*, 2021, **36**, 1201–1209.

Please do not adjust margins

18 S. K. I. Funke, C. Factor, M. Rasschaert, L. Lezius, M. Sperling, U. Karst and P. Robert, *Radiology*, 2022, **305**, 179–189.
19 P. Yamkate, S. Funke, K. Steiger, R. M. Gold, J. A. Lidbury, U. Karst and J. M. Steiner, *J. Feline Med. Surg.*, 2023, **25**, 1098612X231186919.
20 R. González De Vega, M. L. Fernández-Sánchez, J. Pisonero, N. Eiró, F. J. Vizoso and A. Sanz-Medel, *J. Anal. At. Spectrom.*, 2017, **32**, 671–677.
21 L. Qiu, D. Kang, C. Wang, W. Guo, F. Fu, Q. Wu, G. Xi, J. He, L. Zheng, Q. Zhang, X. Liao, L. Li, J. Chen and H. Tu, *Nat. Commun.*, 2022, **13**, 4250.
22 D. P. Bishop, D. Clases, F. Fryer, E. Williams, S. Wilkins, D. J. Hare, N. Cole, U. Karst and P. A. Doble, *J. Anal. At. Spectrom.*, 2016, **31**, 197–202.
23 T. Van Acker, S. Theiner, E. Bolea-Fernandez, F. Vanhaecke and G. Koellensperger, *Nat. Rev. Methods Primer*, 2023, **3**, 52.
24 M. Vázquez Peláez, J. M. Costa-Fernández and A. Sanz-Medel, *J Anal Spectrom*, 2002, **17**, 950–957.
25 D. Savard, S. Dare, L. P. Bédard and S. Barnes, *Geostand. Geoanalytical Res.*, 2023, **47**, 243–265.
26 T. E. Lockwood, R. Gonzalez De Vega, Z. Du, L. Schlatt, X. Xu and D. Clases, *J. Anal. At. Spectrom.*, 2024, 10.1039.D3JA00288H.
27 J. T. Van Elteren, V. S. Šelih and M. Šala, *J. Anal. At. Spectrom.*, 2019, **34**, 1919–1931.
28 M. T. Westerhausen, T. E. Lockwood, R. Gonzalez De Vega, A. Röhnelt, D. P. Bishop, N. Cole, P. A. Doble and D. Clases, *Analyst*, 2019, **144**, 6881–6888.
29 T. E. Lockwood, M. T. Westerhausen and P. A. Doble, *Anal. Chem.*, 2021, **93**, 10418–10423.
30 A. Y. Vorobyev and C. Guo, *J. Phys. Conf. Ser.*, 2007, **59**, 418–423.

